Electrocatalytic Hydrogen Evolution with a Cobalt Complex Bearing Pendant Proton Relays: Acid Strength and Applied Potential Govern Mechanism and Stability

Nicolas Queyriaux, Dongyue Sun, Jennifer Fize, Jacques Pécaut, Martin J. Field, Murielle Chavarot-Kerlidou, Vincent Artero

Electrocatalytic Hydrogen Evolution with a Cobalt Complex Bearing Pendant Proton Relays: Acid Strength and Applied Potential Govern Mechanism and Stability

Nicolas Queyriaux,[a*] Dongyue Sun,[a] Jennifer Fize,[a] Jacques Pécaut,[b] Martin J. Field,[a] Murielle Chavarot-Kerlidou[a] and Vincent Artero[a*]

a - Univ. Grenoble Alpes, CNRS, CEA, IRIG, Laboratoire de Chimie et Biologie des Métaux, UMR 5249, 17 rue des Martyrs, 38000 Grenoble, France.

b - Univ. Grenoble Alpes, CEA, CNRS, IRIG, SYMMES, UMR 5819 Equipe Chimie Interface Biologie pour l'Environnement la Santé et la Toxicologie, F-38054, Grenoble Cedex 9, France.

Abstract. $[Co(bapbpy)Cl]^+$ (*bapbpy*: 6,6'-bis-(2-aminopyridyl)-2,2'-bipyridine) is a polypyridyl cobalt(II) complex bearing both a redox-active bipyridine ligand and pendant proton relays. This compound catalyzes electro-assisted H_2 evolution in DMF with distinct mechanisms depending on the strength of the acid used as the proton source (pKa values ranging from 3.4 to 13.5 in DMF) and the applied potential. Electrochemical studies combining cyclic voltammetry and bulk electrolysis measurements enabled to bring out four distinct catalytic processes. Where applicable, relevant kinetic information were obtained using either foot-of-the-wave analysis (FOWA) or analytical treatment of bulk electrolysis experiments. Among the different catalytic pathways identified in this study, a clear relationship between the catalyst performances and stability was evidenced. These results draw attention to a number of interesting considerations and may help in the development of future adequately-designed catalysts.

Introduction

Hydrogen (H_2) evolved from water through proton reduction appears as an appealing sustainable energy carrier, potentially capable for substituting current carbon-based fuels. The development of cheap H_2-evolving molecular catalysts based on abundant transition metals[1-6] is thus the subject of intense research activity. Current challenges include the design of new catalytic platforms featuring higher activity together with increased stability. Introduction of proton relays in the second coordination sphere of the metal center[7-9] or redox-active ligands[10-14] have been proved essential to promote, tune or enhance catalytic activity. Notable examples involve the control of the formation of cobalt-hydride derivatives as the key active species in catalysis.[15-20] Recently, cobalt(II) polypyridyl complexes have emerged as promising catalysts for hydrogen evolution. Such ligand platforms offer high robustness thanks to their ability to stabilize low oxidation states of the metal centers involved in the catalytic cycle[21-22] and their resistance to hydrogenation. Indeed, intramolecular hydride transfers have been proposed as a likely cause for the deactivation of catalysts from the well-known cobaloxime family.[23-24]

It has recently been stressed out that the optimization of catalytic performances does not only rely on the tuning of the electronic properties of the starting (pre)catalysts but also requires manipulating mechanistic pathways, thus affecting the nature of the active species.[25] By using a complex displaying potential bifurcations in its catalytic pathways due to its proton- and redox-responsive ligand platform, it becomes possible to compare different routes by simply tuning the catalytic conditions (pKa of the acid, applied potential). Herein, we describe how catalytic potential and strength of the proton source affect the reactivity of a cobalt(II)-polypyridyl catalyst[26] combining pendant bases and redox-active ligand. Using analytical electrochemical tools,[27-28] four distinct catalytic pathways for hydrogen evolution, involving different cobalt-hydride intermediates, have been identified. For the first time, the impact of the

nature of these intermediates on both the rate and stability of the catalytic processes has been determined.

Results and discussion

Synthesis, UV-vis properties and structural information.

Metalation of the 6,6'-bis-(2-aminopyridyl)-2,2'-bipyridine (*bapbpy*) ligand[29-30] with $CoCl_2.6H_2O$ in methanol yields the chloride salt of $[Co(bapbpy)Cl]^+$ (Figure 1, $\mathbf{Co^{II}L}$) as a yellow powder. This complex is soluble in aprotic polar solvents such as acetone, CH_3CN, DMF but only poorly soluble in water. In methanol, the UV-vis absorption spectrum of $\mathbf{Co^{II}L}$ is dominated by π-π^* and intra-ligand charge transfer transitions (Figure S1 and Table S1). Noticeably, it also displays a shoulder at 410 nm, assigned to a d-d transition.[31] The X-ray structure of $\mathbf{Co^{II}L}$ shows a strongly distorted trigonal bipyramidal geometry ($\tau = 0.55$)[32, 33] with one pyridine ring and the bipyridine moiety in the equatorial plane. The coordination sphere is complemented by the second pyridine ring sitting slightly outside the plane and a pseudo-axial chloride ligand (Figure 1 and Table S2 for selected bond lengths and angles). This saddle-shape structure appears similar to the previously reported zinc(II) *bapbpy* complex.[30] The amino groups of the *bapbpy* ligand are not bound to the Co^{II} center and are therefore free to act as proton relays during catalysis.

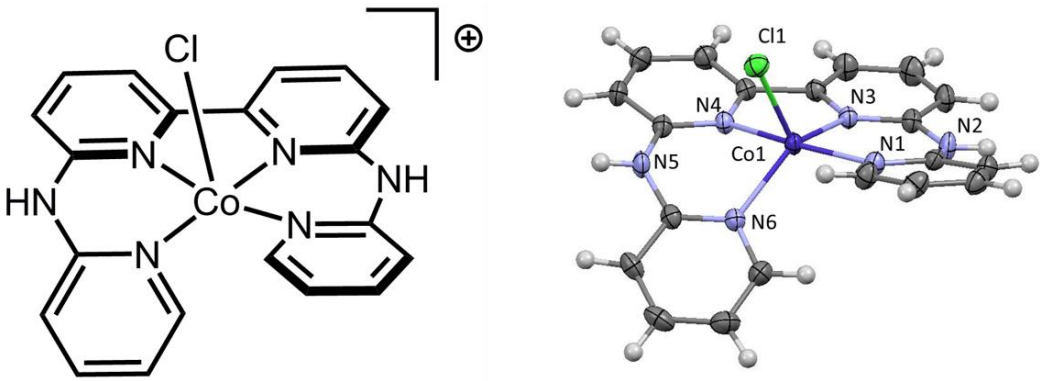

Figure 1. Structure of $[Co(bapbpy)Cl]^+$ ($\mathbf{Co^{II}L}$) in $[Co(bapbpy)Cl]Cl{\cdot}MeOH$ with thermal ellipsoids at the 70% probability level. Chloride counterion and non-coordinating solvent molecules were omitted for sake of clarity.

Electrochemical properties.

The cyclic voltammogram of **$Co^{II}L$** recorded at a glassy carbon (GC) electrode in DMF displays quasi-reversible redox processes at –0.11 V (ΔE = 136 mV) and –1.44 V (ΔE = 76 mV) *vs* Fc^+/Fc, respectively assigned to the Co^{III}/Co^{II} and Co^{II}/Co^{I} couples on the basis of previous literature data (Figure 2 and Table S3).[15, 34-36] The broadness of the wave associated with the $Co^{III/II}$ couple is an expected feature of this class of compounds[36-37] and is likely due to a slow interfacial electron transfer kinetics related to structural reorganization from high-spin Co^{II} complex to a potentially low-spin Co^{III} compound.[37] By contrast, the well-defined and reversible Co^{II}/Co^{I} couple supports low structural reorganization: upon reduction, chloride loss is precluded on the timescale of cyclic voltammetry. When swept to more cathodic potentials, a poorly reversible wave is observed at –1.99 V *vs* Fc^+/Fc. We assign this redox event to a ligand-based process from comparison with the CV of the *bapbpy* complex of the redox-inactive zinc(II) ion that displays a similar wave at –1.96 V *vs* Fc^+/Fc (Figure 2). DFT calculations further support this assignment to a **$Co^{I}(L^{\bullet-})$** species, the spin density of this S= ½ species being mainly centered on the bipyridine moiety of the *bapbpy* ligand (Tables S4-S6). The poor reversibility is likely due to chloride elimination upon reduction, a process that was calculated as thermodynamically favorable.

In order to obtain a full picture of the system, we sought to obtain quantitative data best describing its electrochemical behavior. Using the Randles-Sevcik equation, the catalyst diffusion coefficient was determined through a variable scan rate study, affording a value of 3 $\times 10^{-6}$ $cm^2.s^{-1}$, in line with related molecular cobalt complexes (see the Supporting Information for more details).[17, 38-40] Interestingly, when plotting the variation of the anodic and cathodic peak potentials ($E_{p,a}$ and $E_{p,c}$) for the two cobalt-centered processes *versus* the logarithm of the scan rate (ranging from 100 $mV.s^{-1}$ to 2000 $mV.s^{-1}$), linear trends are observed. Equivalent slopes of opposite signs (+20 and –20 $mV.dec^{-1}$) were determined for the $Co^{II/I}$ couple (Figure

S2). By contrast, unbalanced results were obtained in the case of the $Co^{III/II}$ couple (+90 and – 35 $mV.dec^{-1}$), highlighting an asymmetry of the energy barrier for electron transfer.

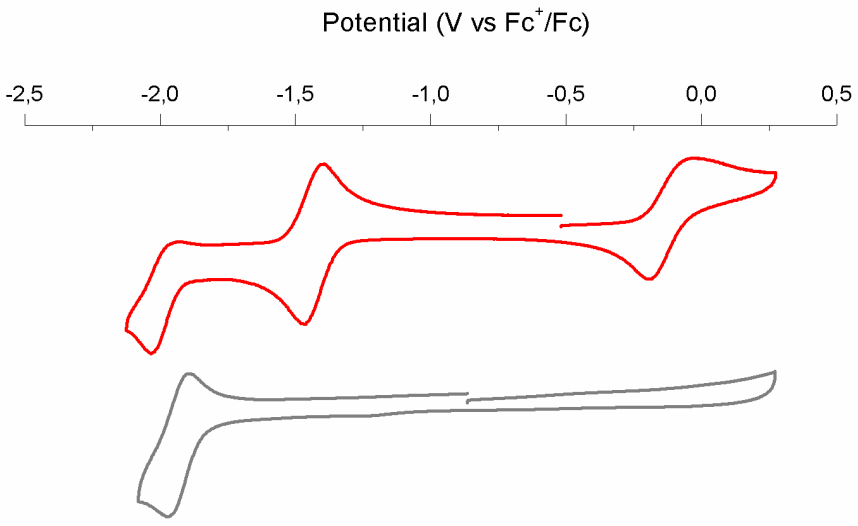

Figure 2. Cyclic voltammograms of **$Co^{II}L$**, (1 mM, red trace) and $[Zn(bapbpy)Cl]^+$ (1 mM, grey trace) recorded in DMF (0.1 M nBu$_4$NBF$_4$) at a glassy carbon electrode and 100 $mV.s^{-1}$.

Acid-base properties.

Knowing the pK_a values associated with **$Co^{II}L$** is important for better understanding the protonation states that can be reached by the catalyst in the absence of any reductive process, *i.e.* the nature of the entry point in the catalytic cycle. We thus performed UV-Vis titration of **$Co^{II}L$** in the presence of increasing amounts of trifluoromethanesulfonic acid (TfOH) in DMF (See Figure S3-S4 and associated paragraph in the Supporting Information for more details). The total dissociation of TfOH in DMF allowed direct measurements of the two first pK_as associated with the cobalt catalyst at 6.3 (**$Co^{II}L/Co^{II}LH^+$**) and 0.8 (**$Co^{II}LH^+/Co^{II}LH_2^{2+}$**). Relevant ligand pKa values to compare with are rare in the literature. pKa of well-studied nickel-phosphine compounds for which the role of pendant bases has been widely investigated by DuBois and Bullock are ranging from 6 to 14 in CH_3CN, depending on the protonation site and overall conformation of the complex.[41] Similarly, Marinescu and Miller recently reported pKa values ranging between 2 and 4 for related cobalt polypyridyl complexes capable to selectively electro-assist CO_2-to-CO conversion in CH_3CN.[9] It should be noted that the pKa

scale is shrunk in DMF compared to CH_3CN, with for example the pKa of $HNEt_3^+$ being 9 units higher in CH_3CN than in DMF.[42] Therefore the bapbpy ligand in **$Co^{II}L$** can behave as a base of similar strength than trifluoroacetate in DMF.[43]

Electrocatalytic properties and mechanistic investigations.

Investigation of the electrocatalytic activity of **$Co^{II}L$** toward hydrogen evolution was then performed in DMF. While a similar complex has already been shown active for H_2 evolution under electro-assisted conditions in aqueous media,[26] the use of an organic solvent allows for precise monitoring of the proton delivery to the catalytic system by the control of the pKa and the concentration of the proton sources. This approach enables easier investigations on the mechanism pathways followed by the catalytic system. Three proton sources with distinct pKa values in this solvent were thus selected:[42] tetrafluoroboric acid HBF_4 (pKa = 3.4), triethylammonium $HNEt_3^+$ (BF_4^- salt, pKa = 9.3) and acetic acid CH_3COOH (pKa = 13.5). CVs of those acids in DMF have been recorded and are displayed in Figure S5-7. Whereas tetrafluoroboric acid and triethylammonium are not known to undergo homoconjugation in DMF,[44] such process could potentially impact acetic acid and slightly reduce the apparent acidity of this proton source. Interestingly, switching from one acid to another allowed very distinct electrocatalytic behaviors to be observed, as detailed in the following.

Electrocatalytic properties and mechanistic investigations: weak acids.

Figure 3 shows the cyclic voltammograms of **$Co^{II}L$** in the presence of increasing amounts of $HNEt_3^+$. The addition of acid triggers the development of a "peak-shaped" catalytic wave with a half-wave potential of –1.90 V vs Fc^+/Fc, regardless of acid concentration. The catalytic peak current is both proportional to the acid concentration and the square root of the scan rate, indicating that the catalytic process is diffusion-limited (Figure S8). Bulk electrolysis confirmed this wave to correspond to catalytic H_2 evolution (Table 1 and S10). In parallel with the appearance of this electrocatalytic wave, it is worth noting that the Co^{II}/Co^{I} couple is

progressively shifted towards anodic potential upon acid addition (Figure 3, process 1). This observation clearly evidences a coupled chemical reaction, here a protonation.[45] Although the pKa of triethylammonium does not allow the protonation of $\mathbf{Co^{II}L}$, the increased electronic density of the one-electron reduced species $\mathbf{Co^{I}L}$ on N2 and N5 (Tables S4 and S5) is likely to trigger *bapbpy* ligand protonation. Interestingly, the electrochemical system remains reversible, indicative of a fast and equilibrated protonation reaction. Under these conditions, a linear increase of the reduction potential of 32 ± 2 mV per decade was observed (Figure S9). In the absence of any modifications in the shape and intensity of the wave associated with the Co^{II}/Co^{I} couple, such behaviour cannot be ascribed to a $2e^-/1H^+$ process. Although not canonical, such a non-ideal behavior is not unprecedented for a proton-coupled electron transfer (PCET)[46] and may reflect a low equilibrium constant or complex equilibria that occur in non-aqueous solvent.[44, 47]

From these results, we propose that catalysis follows an ECEC mechanism (where E corresponds to an electron transfer step and C to a chemical reaction, here protonation): once reduced to $\mathbf{Co^{I}L}$, protonation rapidly occurs at an amino group of the *bapbpy* ligand to form $\mathbf{Co^{I}(LH^{+})}$.[48] The latter is easier to reduce than $\mathbf{Co^{I}L}$, accounting for the 100 mV anodic shift of the catalytic onset potential compared to the ligand-centered process measured in the absence of acid (Figure 3, process 2). Further reduction of $\mathbf{Co^{I}(LH^{+})}$ to $\mathbf{Co^{I}(LH^{\cdot})}$, followed by protonation to form the bis-protonated $\mathbf{Co^{II}H(LH^{+})}$ species, the nature of which will be discussed below, finally allows H_2 to be evolved. Based on such a mechanism, kinetically controlled by the second protonation step, foot-of-the-wave analysis (FOWA)[49-50] allowed the determination of a second order kinetic rate constant of $1.3 \pm 0.1\ 10^5\ M^{-1}.s^{-1}$ for the protonation of $\mathbf{Co^{I}(LH^{\cdot})}$ (see the Supporting information, Table S9 and Figure S10). Controlled-potential electrolysis (CPE) performed at –2.00 V vs Fc^+/Fc (Table 1 and S10) allowed a second-order rate constant value of $2.9 \pm 0.1\ 10^4\ M^{-1}.s^{-1}$, associated with the protonation of $\mathbf{Co^{I}(LH^{\cdot})}$ to be

evaluated.[51] This value is ~4.5 times lower than that the one calculated from the FOWA. We relate this apparent discrepancy to ohmic drop, which more significantly biases CPE than CV measurements.

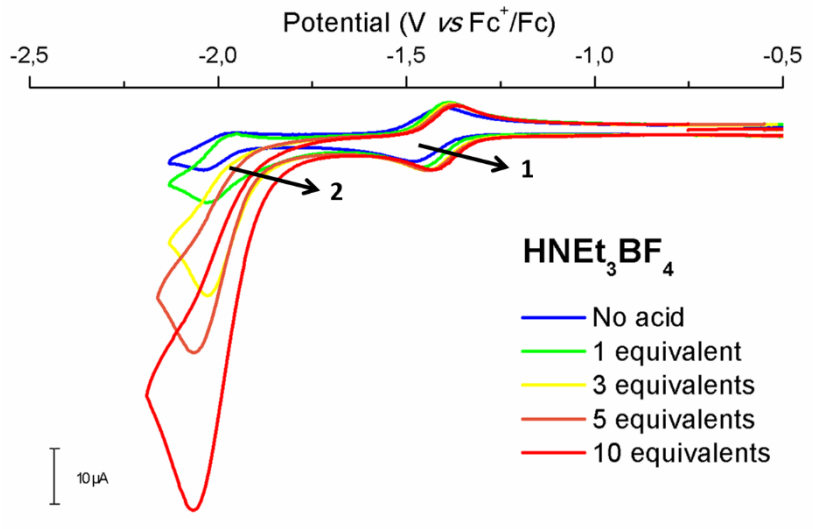

Figure 3 Cyclic voltammograms of **Co^{II}L** (1 mM) recorded in the absence (blue trace) or in the presence of $HNEt_3BF_4$: 1 equivalent (green trace), 3 equivalents (yellow trace), 5 equivalents (orange trace) and 10 equivalents (red trace) in DMF (0.1 M nBu$_4$NBF$_4$) at a glassy carbon electrode and 100 mV.s^{-1}.

When the weaker acetic acid is used as the proton source (pKa = 13.5 in DMF), CVs only display a slight increase in current in the vicinity of the ligand-centered process (Figure S11). However, bulk electrolysis experiments demonstrated that H_2 evolution can also be observed. The absence of any significant anodic shift of the Co^{II}/Co^{I} process when the concentration of acid is progressively increased appears as an evidence of the inability of AcOH to protonate the *bapbpy* ligand in **Co^{I}L**. On the contrary, a ~10 mV cathodic shift is observed, which may point to some ligand exchange process in **Co^{II}L**, as similarly identified on related pentapyridine cobalt(II).[52] To further investigate this hypothesis, the CV of **Co^{II}L** in the presence of sodium acetate (10 mM) have been recorded (Figure S11), displaying a ~150 mV cathodic shift of the potential associated with the Co^{II}/Co^{I} process. The partial dissociation of acetic acid in DMF results in the presence of acetate ions thus capable to efficiently bind **Co^{II}L** complex. Unlike what is observed in the case of triethylammonium addition, no anodic shift of the catalytic onset

potential was identified upon addition of acetic acid. Although acetate binding will likely impact the $Co^{I}L/Co^{I}(L^{\cdot-})$ redox potential, the shift should remain similar to that of the Co^{II}/Co^{I} process until a significant amount of acetate is produced concomitantly to H_2 evolution. Collectively, these data suggest that the increased electronic density of **$Co^{I}L$** is insufficient to allow *bapbpy* ligand protonation by acetic acid. An EECC mechanism passing through the double protonation of the two-electron reduced **$Co^{I}(L^{\cdot-})$** species can thus be assumed in the presence of such a poor proton source in DMF.

Electrocatalytic properties and mechanistic investigations: strong acid.

A drastic change in the electrocatalytic response is observed when HBF_4 is used as the proton source (Figure 4). The Co^{II}/Co^{I} process now becomes irreversible and its cathodic peak potential is gradually shifted towards more positive potentials (Figure 4, process 1). Plotting this variation as a function of the logarithm of the acid concentration provides a linear trace with a slope of 37 ± 1 mV per decade (Figure S12). Associated with the loss of reversibility, this value, in line with the expected value of 29 mV per decade, strongly evidenced an irreversible EC process with fully displaced protonation equilibrium.[53] Considering the relative pKa values of the unreduced complex **$Co^{II}L$** and HBF_4, this $1e^{-}/1H^{+}$ sequence occurs on an already protonated **$Co^{II}(LH^{+})$** complex, thus either leading to the formation of a doubly ligand-protonated Co^{I} complex **$Co^{I}(LH_2^{2+})$** or a protonated Co^{III} hydride species **$Co^{III}H(LH^{+})$**.[53] There are two important elements to preferentially support protonation at the metal center and thus the generation of **$Co^{III}H(LH^{+})$**: (i) the appearance of a new catalytic process at slightly more cathodic potential (*vide infra*) and (ii) calculations performed on cobaloximes that concludes Co^{III} hydrides formation is thermodynamically favored over protonated Co^{I} derivatives (see figure 2 of ref. [54]).

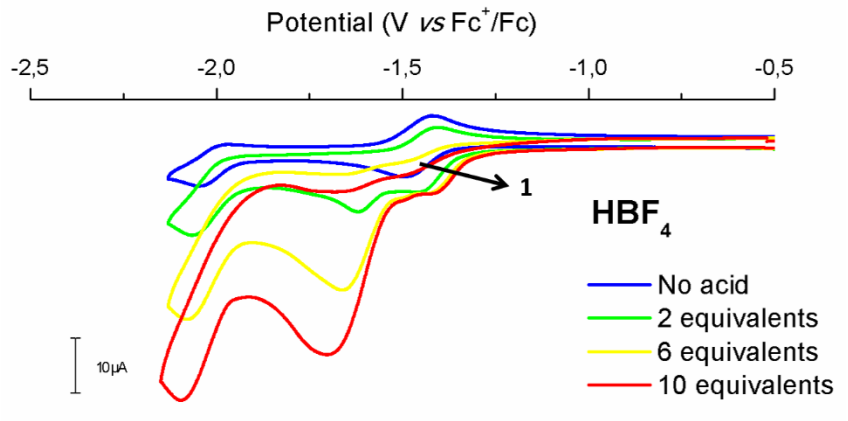

Figure 4. Cyclic voltammograms of **$Co^{II}L$** (1 mM) recorded in the absence (blue trace) or in the presence of HBF_4: 2 equivalent (green trace), 6 equivalents (yellow trace) and 10 equivalents (red trace) in DMF (0.1 M nBu$_4$NBF$_4$) at a glassy carbon electrode and 100 mV.s^{-1}.

In addition to the first process described above, the cyclic voltammograms of **$Co^{II}L$** in the presence of HBF_4 (Figure 4) display two proton-dependent waves with half-wave potentials at –1.65 and –1.90 V *vs* Fc^+/Fc. The latter is reminiscent of the ligand-centered catalytic process observed with $HNEt_3^+$ as proton source. The first one develops at a potential intermediate between those of the Co^{II}/Co^{I} couple and the ligand-based process. Such a catalytic wave likely involves the reduction of the ligand-protonated Co^{III} hydride **$Co^{III}H(LH^+)$** formed after the first reduction process) into a ligand-protonated Co^{II} hydride species, **$Co^{II}H(LH^+)$**, capable of H_2 evolution. The potential of the **$Co^{III}H(LH^+)/Co^{II}H(LH^+)$** couple can thus be estimated to be close to – 1.65 V *vs* Fc^+/Fc, *i.e.* more cathodic than the Co^{II}/Co^{I} couple. This behavior contrasts with the situation found for cobaloximes,[55-56] but is similar to what was established for cobalt complexes bearing ligands that are able to stabilize low Co oxidation states,[57-59] a property shared by polypyridine ligands.[21-22, 60] Due to the close proximity of the irreversible **$Co^{II}(LH^+)/Co^{III}H(LH^+)$** PCET process at the foot of the catalytic wave, FOWA could not be safely applied. Maximal turnover frequencies of ~760 ± 20 s^{-1} and a second order rate constant of 7.6 ± 0.2 10^3 $M^{-1}.s^{-1}$ were therefore extracted from CPE experiments (See the Supporting Information, Tables 1 and S10).[49-51, 61]

The ligand-protonated Co^{II} hydride species **$Co^{II}H(LH^+)$** thus revealed as a potentially crucial intermediate, involved in the electro-assisted H_2 evolution triggered by the presence of $HNEt_3^+$ or HBF_4 (either through the protonation of **$Co^{I}(LH^{\cdot})$** at the metal center or the reduction of **$Co^{III}H(LH^+)$**). DFT calculations of such a bis-protonated species[62] have been undertaken, highlighting the potentially prominent role played by the amino groups to bring together the cobalt hydride and a proton (Figure 5 and Tables S7-S8). Intramolecular protonation of the cobalt hydride by a pendant amino group is indeed favored in **$Co^{II}H(LH^+)$** by a short Co-H···H-N distance (1.57 Å, Figure 5 and Table S11), reminiscent of that found in the active site of hydrogenases[63-64] and some of their mimics that bear a pendant basic site.[65-69] A quick look at the different DFT-calculated structures seems to indicate a certain flexibility of the *bapbpy* ligand that can accommodate various coordination geometries. We provide in the Supporting Information an analysis of the various geometries found in the calculated structures. Although all structures are highly distorted, a major change in coordination mode is found in **$Co^{II}H(LH^+)$**. A pyridine ring indeed adopts an axial position, leaving the equatorial position to the hydride ligand (Figure 5) and thus allowing for a significantly reduced distance between the hydride and the proton born by the amine function of the *bapbpy* ligand.

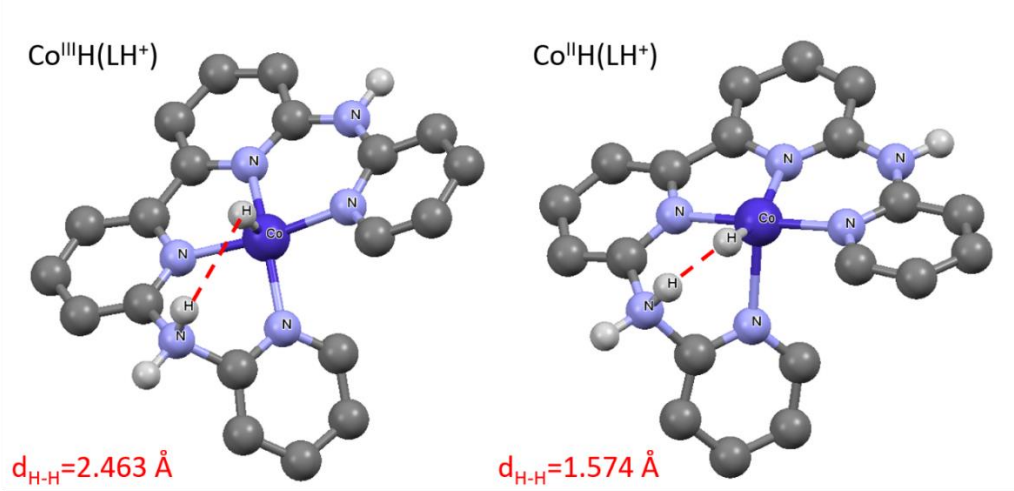

Figure 5. DFT-calculated structures of the relevant bis-protonated **$Co^{III}H(LH^+)$** and **$Co^{II}H(LH^+)$** intermediates. For sake of clarity, aromatic hydrogens have been omitted.

It is worth noting that the peak current related to the **$Co^{II}(LH^{+})$/$Co^{III}H(LH^{+})$** couple measured in the presence of HBF_4 is ~1.5 higher than that of the Co^{II}/Co^{I} process measured in the absence of acid. This value is significantly higher than the expected 1.11 increase for a transition from a pure electron transfer E to an irreversible EC process and might conceal some catalytic activity.[45] Bulk electrolysis was thus run at –1.35 V *vs* Fc^{+}/Fc and demonstrated that H_2 evolution is observed at this potential (Table 1), whereas blank experiment deprived from the cobalt catalyst were unable to yield any hydrogen gas. This catalytic process supports the formation of the Co^{III} hydride species **$Co^{III}H(LH^{+})$**. Homolytic H_2 evolution was formerly described by Gray and coworkers for a related cobalt catalyst.[58] However, the current measured at the peak/plateau linearly depends on the catalyst concentration in the 0.3-3.0 mM range (Figure S13) whereas the mid-wave potential remains unaffected by variation of the catalyst concentration, ruling out homolytic H_2 evolution with non-steady-state concentration of the catalytic intermediate (HON zone).[50, 61] The catalytic current is also not significantly affected by the acid concentration, ruling out both classical heterolytic mechanisms[50] and homolytic mechanism with steady-state concentration of the catalytic intermediate (HOS zone).[61] A possible mechanism to explain such a behavior involves intramolecular proton-hydride coupling as the rate-determining step, as already observed for cobaloximes[70] and DuBois' nickel complexes.[71] In good agreement, DFT calculation revealed a long Co-H···H-N distance of 2.463 Å in **$Co^{III}H(LH^{+})$**) (Figure 5 and Table S11), accounting for the low rate of H_2 evolution measured under these conditions (a TOF of $110 \pm 20\ s^{-1}$, in this case directly equating with the rate-determining first-order constant, was determined from the bulk electrolysis data, Table 1 and Table S10).

Depending on the strength of the acid used and the applied potentials, four distinct catalytic pathways are therefore proposed for **$Co^{II}L$**, respectively triggered by the **$Co^{II}(LH^{+})/Co^{III}H(LH^{+})$**, **$Co^{III}H(LH^{+})/Co^{II}H(LH^{+})$**, **$Co^{I}(LH^{+})/Co^{I}(LH^{\cdot})$** and **$Co^{I}L/Co^{I}(L^{\cdot-})$**

processes (Figure 6). They all involve cobalt-hydride intermediates. Such intermediates may exist as tautomeric forms[72-73] and are often difficult to isolate[39, 74] because of their intrinsic transience and reactivity. Metal hydrides are nevertheless considered as ubiquitous active species for H_2 evolution, not only in synthetic molecular systems, but also in biology[63] and materials science.[75]

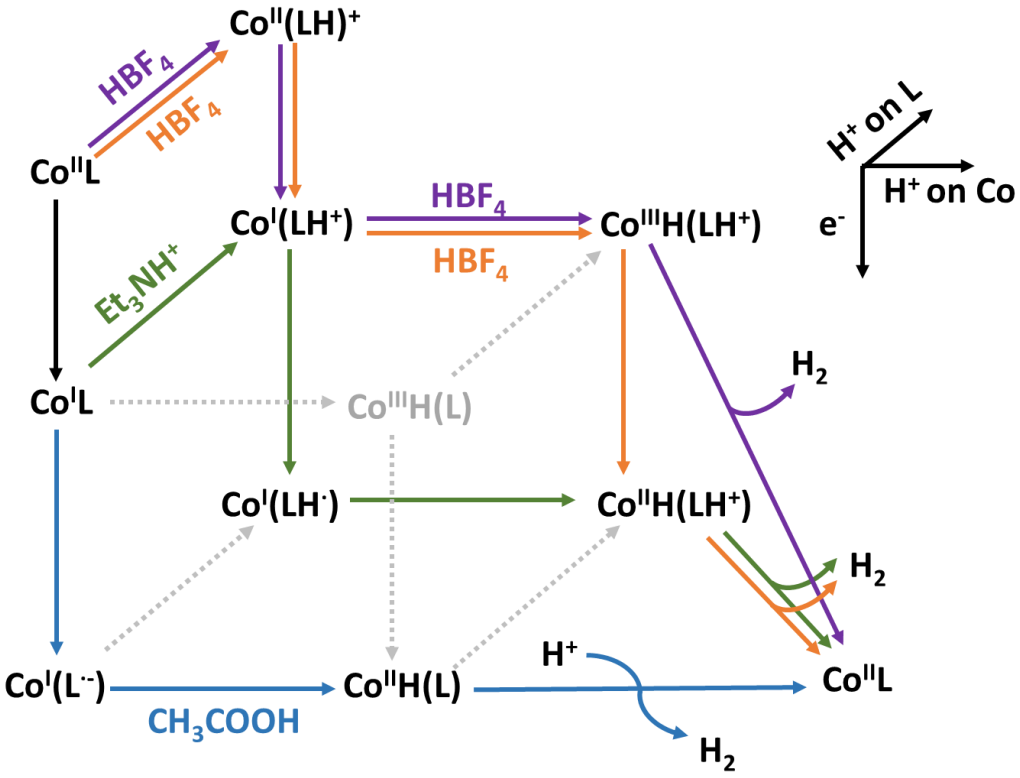

Figure 6. Proposed mechanistic pathways followed by complex **Co^{II}L** during electro-assisted H_2-evolution in the presence of acids of various strengths (blue: AcOH at –2.0 V vs Fc^+/Fc; green: $HNEt_3^+$ and HBF_4 at –1.9 V vs Fc^+/Fc; orange: HBF_4 at –1.65 V vs Fc^+/Fc; purple: HBF_4 at –1.35 V vs Fc^+/Fc) in DMF.

The "catalytic Tafel plot" relating turnover frequency (TOF) and driving force (or overpotential, η)[76] for H_2 evolution shown in Figure 7 benchmarks the performance of the **Co^{II}L** complex for H_2 evolution with those of previously reported catalysts. To build this plot, we used catalytic rate constants extracted from FOWA or bulk electrolysis experiments as detailed previously. The overpotential requirement[44] measured at the half-wave potential of the

catalytic process is reported in Table 1, with errors estimated to 50 mV because of the various tabulated values for the standard potential for the reduction of protons in the solvent considered.[44, 77] The overpotential requirement roughly corresponds to that of change in slope in catalytic Tafel plots. Although not competitive with cobaloximes[78] or DuBois' bioinspired Ni complexes,[79] **Co^{II}L** compares well with other noble-metal free electrocatalysts, such as Fe(TPP)[80] (TPP: tetraphenylporphyrin).

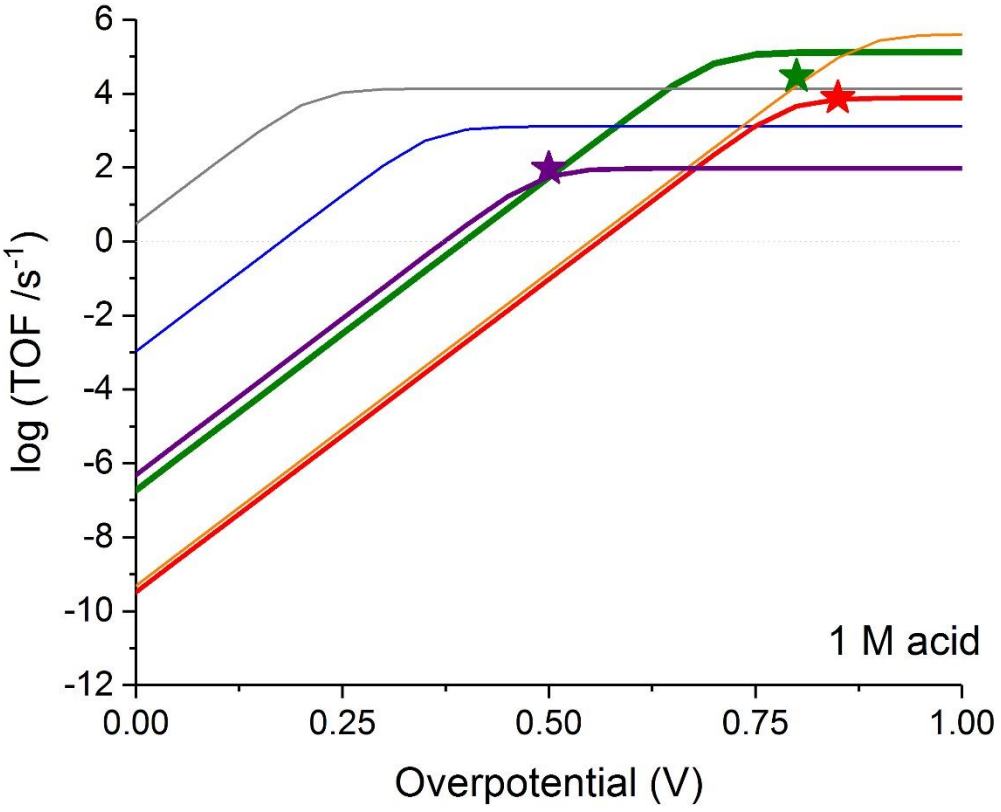

Figure 7. Catalytic Tafel plots relating turnover frequency (s^{-1}) and driving force of H_2 evolution of **Co^{II}L** in the presence of 1M $HNEt_3^+$ (bold green trace) or 1 M HBF_4 (bold red and purple traces for the processes observed at –1.65 V and –1.35 V vs Fc^+/Fc, respectively) with previously reported H_2-evolving electrocatalysts: $[Co(dmgH)_2(py)]$ (grey trace), $[Ni(P_2^{Ph}N_2^{C6H4CH2P(O)(OEt)2})_2]^{2+}$ (blue trace) and [Fe(TPP)Cl] (orange trace). The colored stars indicate TOF values calculated from CPE experiments.

Stability is another crucial factor for an electrocatalyst, in addition to kinetic and overpotential requirements. Savéant and co-workers described how to determine stability-related constants

of electrocatalytic systems from the fit of the charge passed during bulk electrolysis experiments using *equation 1*, in which q_{lim} reflects the charge passed when the catalysts has reached its total turnover number.[81] The t_{chem} values associated with three of the proposed mechanisms are reported in Table 1. t_{chem} can be construed as the lifetime of the catalyst in the diffusion layer, under the considered operating conditions.

$$q(t) = q_{lim}\left[1 - e^{-t/t_{chem}}\right] \qquad \textit{equation 1}$$

In the presence of strong acid, t_{chem} is more than three times lower at –1.65 V *vs* Fc^+/Fc (t_{chem} = 230 ± 15 min) than at –1.35 V *vs* Fc^+/Fc (t_{chem} = 830 ± 25 min). When the weaker $HNEt_3^+$ is used as the proton source, the time constant proves to be even lower (t_{chem} = 90 ± 10 min). Interestingly, the catalyst stability appears as directly related to the potential required to form the active species driving catalysis. The generation of highly-reduced reactive intermediates – such as Co^{II} hydrides or ligand-reduced species – significantly alters the overall stability of the catalytic system. On the other hand, the process requiring the lowest driving force confers a higher stability to the molecular systems, in addition to high-energy conversion yields. This is however at the expense of the catalytic rate. In thermal catalysis, the most (re)active catalysts are more likely to deactivate.[82] To the best of our knowledge the present study provides for the first time a quantitative demonstration that this trend also occurs for electro-assisted processes (low t_{chem} values correlate with high rate constants in Table 1). It is also generally observed in thermally-activated processes that, for a given catalyst, deactivation becomes more severe as substrates more difficult to activate are targeted.[83] The catalytic rate indeed drops while the deactivation process remains unchanged. This trend is also observed here, but for the different reasons, specific to electro-assisted catalysis: we indeed observe a lower stability of the catalyst when it catalyzes the reduction of the weakest $HNEt_3^+$ acid compared to HBF_4, but catalytic intermediates with distinct oxidation state are involved. In particular switching to catalytic

intermediates with lower (more negative) redox potential allows activating weaker acids, but this translate in higher rate for deactivation and therefore lower stability.

Table 1. Bulk electrolysis experiments for H_2 evolution catalyzed by **$Co^{II}L$** (1 mM) in DMF (0.1 M *n*-Bu_4NBF_4) in the presence of 100 mM acid, coupled to gas chromatography analysis (determination of total TON). Working electrode: Hg pool (1.23 cm^2). Counter-electrode: Pt wire. Reference electrode: Ag/AgCl. t_{chem} values were determined using *equation 1* to fit the charge passed over the course of bulk electrolysis experiments (Figures S14-16), overpotential requirements were determined at the mid-wave potential of the catalytic process with 10 mM proton source[44] and rate constants were extracted from initial current densities (see the supporting information and Table S10).

Proton source	**Applied Potential** (V *vs* Fc^+/Fc)	**Total Turnover Number** (tTON)	**Faradaic Efficiency**[a] (ρ_F)	**Time Constant**[b] (t_{chem}, min)	**Overpotential requirement** (mV)	**Rate constants** ($M^{-1}. s^{-1}$)
Et_3NH^+	-2.00	28 (± 3)	93 (± 10) %	90 (± 10)	890 (± 50)	$k = 2.9 (\pm 0.1) 10^4$
HBF_4	-1.65	35 (± 12)	72 (± 30) %	230 (± 15)	880 (± 50)	$k = 7.6 (\pm 0.2) 10^3$
HBF_4	-1.35	4 (± 2)	77 (± 30) %	830 (± 25)	580 (± 50)	$k = 1.1 (\pm 0.2) 10^2$

[a] the constant systematic error in the determination of H_2 amount due to the online detection method used here translates into lower faradic efficiencies (%) for lower catalytic current.

[b] additional simulations were performed to estimate the uncertainty on the fit performed to get the t_{chem} values.

Conclusion

Polypyridyl ligands have proved instrumental in the design of stable and water-soluble Co-based H_2-evolving catalysts.[3, 21] The cobalt(II) polypyridyl complex $[Co(bapbpy)Cl]^+$, **$Co^{II}L$**, is one of the rare catalysts for H_2 evolution that features both a redox-active moiety and proton relays, an original combination of features in the Co polypyridyl family of catalysts. Depending

on the acidity of the medium and the operating potential, one or both these features can be exploited to promote catalytic activity, resulting in four identified pathways for H_2 evolution involving either metal-centered and/or ligand-assisted processes. Importantly, we also established a direct relationship between the stability of the catalytic system and the operating potential required to generate the active species, showing that stable intermediates not only confer low overpotential requirement but also higher stability. As **$Co^{II}L$** is active for H_2 evolution in aqueous media,[26] future work in our group will target the implementation of such a catalytic platform into dye-sensitized photoelectrochemical cells for overall water splitting.[84-85]

ASSOCIATED CONTENT

The following files are available free of charge.

Electronic supporting information (PDF): experimental and computational section, additional spectroscopic, electrochemical and structural data, methodology used to extract kinetic and thermodynamic information from electrochemical and spectroscopic data.

AUTHOR INFORMATION

Corresponding Authors

nicolas.queyriaux@lcc-toulouse.fr

vincent.artero@cea.fr

Author Contributions

The manuscript was written through contributions of all authors. All authors have given approval to the final version of the manuscript.

ACKNOWLEDGEMENTS.

This work was supported by the European Research Council and European Commission's Seventh Framework Program (FP7/2007-2013) under grant agreement n° 306398 (project Photocat$\mathbf{H_2}$ode) and the French National Research Agency (Labex Program, ArCANE, ANR-11-LABX-0003-01 and CBH-EUR-GS, ANR-17-EURE-0003). We also thank Dr. Nicolas Kaeffer for fruitful discussion regarding this study.

References.

1. Du, P.; Eisenberg, R., Catalysts made of earth-abundant elements (Co, Ni, Fe) for water splitting: Recent progress and future challenges. *Energy Environ. Sci.* **2012,** *5*, 6012.
2. Artero, V.; Chavarot-Kerlidou, M.; Fontecave, M., Splitting water with cobalt. *Angew Chem Int Ed Engl* **2011,** *50*, 7238-66.
3. McKone, J. R.; Marinescu, S. C.; Brunschwig, B. S.; Winkler, J. R.; Gray, H. B., Earth-abundant hydrogen evolution electrocatalysts. *Chem. Sci.* **2014,** *5*, 865-878.
4. Zee, D. Z.; Chantarojsiri, T.; Long, J. R.; Chang, C. J., Metal-polypyridyl catalysts for electro- and photochemical reduction of water to hydrogen. *Acc. Chem. Res.* **2015,** *48*, 2027-36.
5. Pal, R.; Laureanti, J. A.; Groy, T. L.; Jones, A. K.; Trovitch, R. J., Hydrogen production from water using a bis(imino)pyridine molybdenum electrocatalyst. *Chem. Commun.* **2016,** *52*, 11555-11558
6. Tran, P. D.; Tran, T. V.; Orio, M.; Torelli, S.; Truong, Q. D.; Nayuki, K.; Sasaki, Y.; Chiam, S. Y.; Yi, R.; Honma, I.; Barber, J.; Artero, V., Coordination polymer structure and revisited hydrogen evolution catalytic mechanism for amorphous molybdenum sulfide. *Nat. Mater.* **2016,** *15*, 640-646.
7. Rakowski DuBois, M.; DuBois, D. L., Development of molecular electrocatalysts for CO_2 reduction and H_2 production/oxidation. *Acc. Chem. Res.* **2009,** *42*, 1974-82.
8. Rakowski DuBois, M.; DuBois, D. L., The roles of the first and second coordination spheres in the design of molecular catalysts for H2 production and oxidation. *Chem. Soc. Rev.* **2009,** *38*, 62-72.
9. Chapovetsky, A.; Welborn, M.; Luna, J. M.; Haiges, R.; Miller, T. F.; Marinescu, S. C., Pendant Hydrogen-Bond Donors in Cobalt Catalysts Independently Enhance CO2 Reduction. *ACS Cent. Sci.* **2018,** *4*, 397-404.
10. Haddad, A. Z.; Garabato, B. D.; Kozlowski, P. M.; Buchanan, R. M.; Grapperhaus, C. A., Beyond Metal-Hydrides: Non-Transition-Metal and Metal-Free Ligand-Centered Electrocatalytic Hydrogen Evolution and Hydrogen Oxidation. *J. Am. Chem. Soc.* **2016,** *138*, 7844-7.
11. Solis, B. H.; Maher, A. G.; Dogutan, D. K.; Nocera, D. G.; Hammes-Schiffer, S., Nickel phlorin intermediate formed by proton-coupled electron transfer in hydrogen evolution mechanism. *Proc. Natl. Acad. Sci. USA* **2016,** *113*, 485-492.
12. Dempsey, J. L., Ligand steals spotlight from metal to orchestrate hydrogen production. *Proc. Natl. Acad. Sci. USA* **2016,** *113*, 478-9.
13. Thompson, E. J.; Berben, L. A., Electrocatalytic Hydrogen Production by an Aluminum(III) Complex: Ligand-Based Proton and Electron Transfer. *Angew. Chem. Int. Ed.* **2015,** *54*, 11642-11646.
14. Tok, G. C.; Freiberg, A. T. S.; Gasteiger, H. A.; Hess, C. R., Electrocatalytic H_2 Evolution by the Co-Mabiq Complex Requires Tempering of the Redox-Active Ligand. *ChemCatChem* **2019,** *11*, 3973-3981.
15. Jurss, J. W.; Khnayzer, R. S.; Panetier, J. A.; El Roz, K. A.; Nichols, E. M.; Head-Gordon, M.; Long, J. R.; Castellano, F. N.; Chang, C. J., Bioinspired design of redox-active ligands for multielectron catalysis: effects of positioning pyrazine reservoirs on cobalt for electro- and photocatalytic generation of hydrogen from water. *Chem. Sci.* **2015,** *6*, 4954-4972.
16. Jacobsen, G. M.; Yang, J. Y.; Twamley, B.; Wilson, A. D.; Bullock, R. M.; DuBois, M. R.; DuBois, D. L., Hydrogen production using cobalt-based molecular catalysts containing a proton relay in the second coordination sphere. *Energy Environ. Sci.* **2008,** *1*, 167-174.
17. Roubelakis, M. M.; Bediako, D. K.; Dogutan, D. K.; Nocera, D. G., Proton-coupled electron transfer kinetics for the hydrogen evolution reaction of hangman porphyrins. *Energy Environ. Sci.* **2012,** *5*, 7737-7740.
18. Graham, D. J.; Nocera, D. G., Electrocatalytic H_2 Evolution by Proton-Gated Hangman Iron Porphyrins. *Organometallics* **2014,** *33*, 4994-5001.
19. Wang, P.; Liang, G.; Reddy, M. R.; Long, M.; Driskill, K.; Lyons, C.; Donnadieu, B.; Bollinger, J. C.; Webster, C. E.; Zhao, X., Electronic and Steric Tuning of Catalytic H2 Evolution by Cobalt Complexes with Pentadentate Polypyridyl-Amine Ligands. *J. Am. Chem. Soc.* **2018,** *140*, 9219-9229.
20. Ai, W.; Zhong, R.; Liu, X.; Liu, Q., Hydride Transfer Reactions Catalyzed by Cobalt Complexes. *Chemical Reviews* **2019,** *119*, 2876-2953.
21. Queyriaux, N.; Jane, R. T.; Massin, J.; Artero, V.; Chavarot-Kerlidou, M., Recent developments in hydrogen evolving molecular cobalt(II)–polypyridyl catalysts. *Coord. Chem. Rev.* **2015,** *304–305*, 3-19.
22. Hickey, D. P.; Sandford, C.; Rhodes, Z.; Gensch, T.; Fries, L. R.; Sigman, M. S.; Minteer, S. D., Investigating the Role of Ligand Electronics on Stabilizing Electrocatalytically Relevant Low Valent Co(I) Intermediates. *J. Am. Chem. Soc.* **2019,** *141* 1382-1392.
23. Simandi, L. I.; Szeverenyi, Z.; Budozahonyi, E., Activation of Molecular-Hydrogen by Cobaloxime(II) Derivatives. *Inorg. Nucl. Chem. Lett.* **1975,** *11*, 773-777.
24. Simandi, L. I.; Budo-Zahonyi, E.; Szeverenyi, Z., Effect of strong base on the activation of molecular hydrogen by pyridinebis(dimethylglyoximato)cobalt(II). *Inorg. Nucl. Chem. Lett.* **1976,** *12*, 237-241.
25. Costentin, C.; Savéant, J.-M., Homogeneous Molecular Catalysis of Electrochemical Reactions: Manipulating Intrinsic and Operational Factors for Catalyst Improvement. *J. Am. Chem. Soc.* **2018,** *140*, 16669-16675.
26. Queyriaux, N.; Giannoudis, E.; Windle, C. D.; Roy, S.; Pecaut, J.; Coutsolelos, A. G.; Artero, V.; Chavarot-Kerlidou, M., A noble metal-free photocatalytic system based on a novel cobalt tetrapyridyl catalyst for hydrogen production in fully aqueous medium. *Sustainable Energy & Fuels* **2018,** *2*, 553-557.
27. Lee, K. J.; Elgrishi, N.; Kandemir, B.; Dempsey, J. L., Electrochemical and spectroscopic methods for evaluating molecular electrocatalysts. *Nature Reviews Chemistry* **2017,** *1*, 0039.
28. Sandford, C.; Edwards, M. A.; Klunder, K. J.; Hickey, D. P.; Li, M.; Barman, K.; Sigman, M. S.; White, H. S.; Minteer, S. D., A synthetic chemist's guide to electroanalytical tools for studying reaction mechanisms. *Chem. Sci.* **2019,** *10*, 6404-6422.

29. Bonnet, S.; Siegler, M. A.; Costa, J. S.; Molnar, G.; Bousseksou, A.; Spek, A. L.; Gamez, P.; Reedijk, J., A two-step spin crossover mononuclear iron(II) complex with a [HS-LS-LS] intermediate phase. *Chem. Commun.* **2008**, 5619-21.
30. Molenbroek, E.; Straathof, N.; Duck, S.; Rashid, Z.; van Lenthe, J. H.; Lutz, M.; Gandubert, A.; Klein Gebbink, R. J.; De Cola, L.; Bonnet, S., Zinc coordination to the bapbpy ligand in homogeneous solutions and at liposomes: zinc detection via fluorescence enhancement. *Dalton Trans.* **2013,** *42*, 2973-84.
31. Bacchi, M.; Berggren, G.; Niklas, J.; Veinberg, E.; Mara, M. W.; Shelby, M. L.; Poluektov, O. G.; Chen, L. X.; Tiede, D. M.; Cavazza, C.; Field, M. J.; Fontecave, M.; Artero, V., Cobaloxime-Based Artificial Hydrogenases. *Inorg. Chem.* **2014,** *53*, 8071-8082.
32. Addison, A. W.; Rao, T. N.; Reedijk, J.; van Rijn, J.; Verschoor, G. C., Synthesis, structure, and spectroscopic properties of copper(II) compounds containing nitrogen-sulphur donor ligands; the crystal and molecular structure of aqua[1,7-bis(N-methylbenzimidazol-2'-yl)-2,6-dithiaheptane]copper(II) perchlorate. *J. Chem. Soc., Dalton Trans.* **1984**, 1349-1356.
33. $\tau = (a-b)/60$ with a and b the largest angles in the metal coordination sphere; τ ranges from 0 (perfect square bipyramide) to 1 for a perfect trigonal bipyramid.
34. Lo, W. K. C.; Castillo, C. E.; Gueret, R.; Fortage, J.; Rebarz, M.; Sliwa, M.; Thomas, F.; McAdam, C. J.; Jameson, G. B.; McMorran, D. A.; Crowley, J. D.; Collomb, M.-N.; Blackman, A. G., Synthesis, Characterization, and Photocatalytic H_2-Evolving Activity of a Family of $[Co(N4Py)(X)]^{n+}$ Complexes in Aqueous Solution. *Inorg. Chem.* **2016,** *55*, 4564-4581.
35. Tong, L.; Zong, R.; Thummel, R. P., Visible Light-Driven Hydrogen Evolution from Water Catalyzed by A Molecular Cobalt Complex. *J. Am. Chem. Soc.* **2014,** *136*, 4881-4884.
36. Deponti, E.; Luisa, A.; Natali, M.; Iengo, E.; Scandola, F., Photoinduced hydrogen evolution by a pentapyridine cobalt complex: elucidating some mechanistic aspects. *Dalton Trans.* **2014,** *43*, 16345-16353.
37. Nippe, M.; Khnayzer, R. S.; Panetier, J. A.; Zee, D. Z.; Olaiya, B. S.; Head-Gordon, M.; Chang, C. J.; Castellano, F. N.; Long, J. R., Catalytic proton reduction with transition metal complexes of the redox-active ligand bpy_2PYMe. *Chem. Sci.* **2013,** *4*, 3934-3945.
38. Elgrishi, N.; Kurtz, D. A.; Dempsey, J. L., Reaction Parameters Influencing Cobalt Hydride Formation Kinetics: Implications for Benchmarking H-2-Evolution Catalysts. *J. Am. Chem. Soc.* **2017,** *139*, 239-244.
39. Wiedner, E. S.; Bullock, R. M., Electrochemical Detection of Transient Cobalt Hydride Intermediates of Electrocatalytic Hydrogen Production. *J. Am. Chem. Soc.* **2016,** *138*, 8309-8318.
40. Elgrishi, N.; Chambers, M. B.; Artero, V.; Fontecave, M., Terpyridine complexes of first row transition metals and electrochemical reduction of CO_2 to CO. *Phys. Chem. Chem. Phys.* **2014,** *16*, 13635-13644.
41. Raugei, S.; Chen, S. T.; Ho, M. H.; Ginovska-Pangovska, B.; Rousseau, R. J.; Dupuis, M.; DuBois, D. L.; Bullock, R. M., The Role of Pendant Amines in the Breaking and Forming of Molecular Hydrogen Catalyzed by Nickel Complexes. *Chem. Eur. J.* **2012,** *18*, 6493-6506.
42. Izutsu, K., Acid-Base Dissociation Constants in Dipolar Aprotic Solvents. *Blackwell Scientific: Oxford, U.K.* **1990**.
43. Fourmond, V.; Canaguier, S.; Golly, B.; Field, M. J.; Fontecave, M.; Artero, V., A nickel-manganese catalyst as a biomimic of the active site of NiFe hydrogenases: a combined electrocatalytical and DFT mechanistic study. *Energy Environ. Sci.* **2011,** *4*, 2417-2427.
44. Fourmond, V.; Jacques, P. A.; Fontecave, M.; Artero, V., H_2 evolution and molecular electrocatalysts: determination of overpotentials and effect of homoconjugation. *Inorg. Chem.* **2010,** *49*, 10338-47.
45. Savéant, J.-M., Coupling of Electrode Electron Transfers with Homogeneous Chemical Reactions. In *Elements of Molecular and Biomolecular Electrochemistry*, John Wiley & Sons, Inc.: 2006; pp 78-181.
46. Efros, L. L.; Thorp, H. H.; Brudvig, G. W.; Crabtree, R. H., Towards a functional model of hydrogenase: electrocatalytic reduction of protons to dihydrogen by a nickel macrocyclic complex. *Inorg. Chem.* **1992,** *31*, 1722-1724.
47. McCarthy, B. D.; Dempsey, J. L., Decoding Proton-Coupled Electron Transfer with Potential–pKa Diagrams. *Inorg. Chem.* **2017,** *56*, 1225-1231.
48. Zone DE in the diagram p 81 in Savéant, J. M. Elements of Molecular and Biomolecular Electrochemistry; Wiley, 2006.
49. Costentin, C.; Drouet, S.; Robert, M.; Saveant, J. M., Turnover numbers, turnover frequencies, and overpotential in molecular catalysis of electrochemical reactions. Cyclic voltammetry and preparative-scale electrolysis. *J. Am. Chem. Soc.* **2012,** *134*, 11235-42.
50. Costentin, C.; Savéant, J.-M., Multielectron, Multistep Molecular Catalysis of Electrochemical Reactions: Benchmarking of Homogeneous Catalysts. *ChemElectroChem* **2014,** *1*, 1226-1236.
51. Roy, S.; Sharma, B.; Pécaut, J.; Simon, P.; Fontecave, M.; Tran, P. D.; Derat, E.; Artero, V., Molecular Cobalt Complexes with Pendant Amines for Selective Electrocatalytic Reduction of Carbon Dioxide to Formic Acid. *J. Am. Chem. Soc.* **2017,** *139*, 3685-3696.
52. King, A. E.; Surendranath, Y.; Piro, N. A.; Bigi, J. P.; Long, J. R.; Chang, C. J., A mechanistic study of proton reduction catalyzed by a pentapyridine cobalt complex: evidence for involvement of an anation-based pathway. *Chem. Sci.* **2013,** *4*, 1578-1587.
53. Costentin, C.; Passard, G.; Robert, M.; Savéant, J.-M., Concertedness in proton-coupled electron transfer cleavages of carbon–metal bonds illustrated by the reduction of an alkyl cobalt porphyrin. *Chem. Sci.* **2013,** *4*, 819-823.
54. Solis, B. H.; Yu, Y.; Hammes-Schiffer, S., Effects of Ligand Modification and Protonation on Metal Oxime Hydrogen Evolution Electrocatalysts. *Inorg. Chem.* **2013,** *52*, 6994-6999.
55. Muckerman, J. T.; Fujita, E., Theoretical studies of the mechanism of catalytic hydrogen production by a cobaloxime. *Chem. Commun.* **2011,** *47*, 12456-8.
56. Solis, B. H.; Hammes-Schiffer, S., Theoretical analysis of mechanistic pathways for hydrogen evolution catalyzed by cobaloximes. *Inorg. Chem.* **2011,** *50*, 11252-62.

57. Koelle, U.; Paul, S., Electrochemical reduction of protonated cyclopentadienylcobalt phosphine complexes. *Inorg. Chem.* **1986,** *25*, 2689-2694.
58. Marinescu, S. C.; Winkler, J. R.; Gray, H. B., Molecular mechanisms of cobalt-catalyzed hydrogen evolution. *Proc. Natl. Acad. Sci. USA* **2012,** *109*, 15127-31.
59. Wiedner, E. S.; Appel, A. M.; DuBois, D. L.; Bullock, R. M., Thermochemical and mechanistic studies of electrocatalytic hydrogen production by cobalt complexes containing pendant amines. *Inorg. Chem.* **2013,** *52*, 14391-403.
60. Zee, D. Z.; Chantarojsiri, T.; Long, J. R.; Chang, C. J., Metal–Polypyridyl Catalysts for Electro- and Photochemical Reduction of Water to Hydrogen. *Acc. Chem. Res.* **2015,** *48*, 2027-2036.
61. Costentin, C.; Dridi, H.; Savéant, J.-M., Molecular Catalysis of H_2 Evolution: Diagnosing Heterolytic versus Homolytic Pathways. *J. Am. Chem. Soc.* **2014,** *136*, 13727-13734.
62. DFT calculations showed that in cobalt hydride derivatives, the hydride ligand destabilizes the trans Co-Cl bond, resulting in the elimination of the chloride ligand from the cobalt coordination sphere.
63. Reijerse, E. J.; Pham, C. C.; Pelmenschikov, V.; Gilbert-Wilson, R.; Adamska-Venkatesh, A.; Siebel, J. F.; Gee, L. B.; Yoda, Y.; Tamasaku, K.; Lubitz, W.; Rauchfuss, T. B.; Cramer, S. P., Direct Observation of an Iron-Bound Terminal Hydride in [FeFe]-Hydrogenase by Nuclear Resonance Vibrational Spectroscopy. *J. Am. Chem. Soc.* **2017,** *139*, 4306-4309.
64. Katz, S.; Noth, J.; Horch, M.; Shafaat, H. S.; Happe, T.; Hildebrandt, P.; Zebger, I., Vibrational spectroscopy reveals the initial steps of biological hydrogen evolution. *Chem. Sci.* **2016,** *7*, 6746-6752.
65. Ding, S.; Ghosh, P.; Lunsford, A. M.; Wang, N.; Bhuvanesh, N.; Hall, M. B.; Darensbourg, M. Y., Hemilabile Bridging Thiolates as Proton Shuttles in Bioinspired H_2 Production Electrocatalysts. *J. Am. Chem. Soc.* **2016,** *138*, 12920-12927.
66. Tang, H.; Hall, M. B., Biomimetics of [NiFe]-Hydrogenase: Nickel- or Iron-Centered Proton Reduction Catalysis? *J. Am. Chem. Soc.* **2017,** *139*, 18065-18070.
67. Carroll, M. E.; Barton, B. E.; Rauchfuss, T. B.; Carroll, P. J., Synthetic Models for the Active Site of the [FeFe]-Hydrogenase: Catalytic Proton Reduction and the Structure of the Doubly Protonated Intermediate. *J. Am. Chem. Soc.* **2012,** *134*, 18843-18852.
68. Huynh, M. T.; Schilter, D.; Hammes-Schiffer, S.; Rauchfuss, T. B., Protonation of Nickel-Iron Hydrogenase Models Proceeds after Isomerization at Nickel. *J. Am. Chem. Soc.* **2014,** *136*, 12385-12395.
69. Liu, T.; Wang, X.; Hoffmann, C.; DuBois, D. L.; Bullock, R. M., Heterolytic cleavage of hydrogen by an iron hydrogenase model: an Fe-HH-N dihydrogen bond characterized by neutron diffraction. *Angew Chem Int Ed Engl* **2014,** *53*, 5300-4.
70. Rountree, E. S.; Martin, D. J.; McCarthy, B. D.; Dempsey, J. L., Linear Free Energy Relationships in the Hydrogen Evolution Reaction: Kinetic Analysis of a Cobaloxime Catalyst. *ACS Catal.* **2016,** *6*, 3326-3335.
71. DuBois, D. L., Development of Molecular Electrocatalysts for Energy Storage. *Inorg. Chem.* **2014,** *53*, 3935-3960.
72. Estes, D. P.; Grills, D. C.; Norton, J. R., The Reaction of Cobaloximes with Hydrogen: Products and Thermodynamics. *J. Am. Chem. Soc.* **2014,** *136*, 17362-17365.
73. Bhattacharjee, A.; Chavarot-Kerlidou, M.; Andreiadis, E. S.; Fontecave, M.; Field, M. J.; Artero, V., Combined Experimental-Theoretical Characterization of the Hydrido-Cobaloxime $[HCo(dmgH)_2(P^nBu_3)]$. *Inorg. Chem.* **2012,** *51*, 7087-7093.
74. Lacy, D. C.; Roberts, G. M.; Peters, J. C., The Cobalt Hydride that Never Was: Revisiting Schrauzer's "Hydridocobaloxime". *J. Am. Chem. Soc.* **2015,** *137*, 4860-4864.
75. Copéret, C.; Estes, D. P.; Larmier, K.; Searles, K., Isolated Surface Hydrides: Formation, Structure, and Reactivity. *Chem. Rev.* **2016,** *116*, 8463-8505.
76. Artero, V.; Saveant, J. M., Toward the Rational Benchmarking of Homogeneous H_2-Evolving Catalysts. *Energy Environ Sci* **2014,** *7*, 3808-3814.
77. Roberts, J. A. S.; Bullock, R. M., Direct Determination of Equilibrium Potentials for Hydrogen Oxidation/Production by Open Circuit Potential Measurements in Acetonitrile. *Inorg. Chem.* **2013,** *52*, 3823-3835.
78. Razavet, M.; Artero, V.; Fontecave, M., Proton Electroreduction Catalyzed by Cobaloximes: Functional Models for Hydrogenases. *Inorg. Chem.* **2005,** *44*, 4786-4795.
79. Helm, M. L.; Stewart, M. P.; Bullock, R. M.; DuBois, M. R.; DuBois, D. L., A Synthetic Nickel Electrocatalyst with a Turnover Frequency Above 100,000 s^{-1} for H_2 Production. *Science* **2011,** *333*, 863-866.
80. Bhugun, I.; Lexa, D.; Savéant, J.-M., Homogeneous Catalysis of Electrochemical Hydrogen Evolution by Iron(0) Porphyrins. *J. Am. Chem. Soc.* **1996,** *118*, 3982-3983.
81. Costentin, C.; Passard, G.; Saveant, J. M., Benchmarking of homogeneous electrocatalysts: overpotential, turnover frequency, limiting turnover number. *J. Am. Chem. Soc.* **2015,** *137*, 5461-7.
82. Crabtree, R. H., Deactivation in homogeneous transition metal catalysis: causes, avoidance, and cure. *Chem. Rev.* **2015**, *115,* 127-50.
83. Crabtree, R., Iridium compounds in catalysis. *Acc. Chem. Res.* **1979**, *12*, 331-337.
84. Kaeffer, N.; Massin, J.; Lebrun, C.; Renault, O.; Chavarot-Kerlidou, M.; Artero, V., Covalent Design for Dye-Sensitized H_2-Evolving Photocathodes Based on a Cobalt Diimine–Dioxime Catalyst. *J. Am. Chem. Soc.* **2016,** *138*, 12308-12311.
85. Windle, C.; Kumagai, H.; Higashi, M.; Brisse, R.; Bold, S.; Jousselme, B.; Chavarot-Kerlidou, M.; Maeda, K.; Abe, R.; Ishitani, O.; Artero, V., Earth-Abundant Molecular Z-Scheme Photoelectrochemical Cell for Overall Water-Splitting. *J. Am. Chem. Soc.* **2019**, *141*, 9593-9602.

Graphical Abstract